

InGaN– A NEW SOLAR CELL MATERIAL

Christiana Honsberg, Omkar Jani, Alan Doolittle, Elaissa Trybus, Gon Namkoong Ian Ferguson, David Nicole, Adam Payne
School of Electrical Engineering, Georgia Institute of Technology, Atlanta GA, 30332, USA

ABSTRACT: A fundamental limitation in achieving ultra-high efficiency solar cells ($> 50\%$) is the availability of materials and corresponding device structures. The InGaN material system offer substantial potential in developing ultra-high efficiency devices, both because of measurements indicating that the band gap on InN is lower than previously thought and also due to other unique material properties, such as the strong polarization and piezoelectric effects. Several key issues remain, including p-type doping, which substrates to use, and the material quality of the layers. Modelling results show that the material quality of existing films allows a 5 stack tandem at 500X to approach 50%. Experimental results show InN grown on Ge by MBE with a crystalline Al interlayer, which could be used to replace a tunnel contact. High band gap GaN p-i-n and InGaN/GaN quantum well solar cells are fabricated, showing good spectral response and $V_{oc} > 2V$.

Keywords: High Efficiency, InGaN, InN, tandem

1 INTRODUCTION

The theoretical efficiency limits of solar energy conversion are strongly dependant on the range and number of different band gaps or effective band gaps that can be incorporated into a solar cell. For tandem devices, the range of band gaps available as well as the ability to achieve junctions with specific band gaps and device structures is critical in achieving high efficiency. For alternate approaches, in which one or more of the band gaps are “effective band gaps” due to physical mechanisms such as an intermediate band, higher order excited states, or energy levels or bands introduced by quantum well or quantum dots, the need for specific band gaps is relaxed. However, in both approaches, both the low and the high band gaps are still controlled by the materials system. Consequently, the recent re-measurement of the band gap of InN as on the order of 0.7 eV makes the InGaN alloy system a potential solar cell material.

While band gaps figure prominently in determining efficiency limits, the ability to implement a practical, high efficiency device depends on many other parameters, including absorption, diffusion length, effect of surfaces, lattice constant, and doping. This paper examines the ability to use InGaN for photovoltaic devices with the goal of determining if the InGaN material system can be used to make ultra-high efficiency ($>50\%$ efficiency) solar cells. The advantages of the III-nitride material system are a wide range in band gap, high absorption coefficient, a low effective mass (high mobility), and strong piezoelectric and polarization effects. However, in addition to these advantages, the material system also has significant challenges, some of which are related to the newness of the material (particularly for InN, for which photoluminescence is only measured 2 years ago [1,2,3]), including material quality, defect density, doping, substrates and growth issues.

2 MATERIAL SYSTEMS FOR ULTRA-HIGH EFFICIENCY SOLAR CELLS

The thermodynamic efficiency limits of solar energy conversion, 68.2% at one-sun and 86.8% under maximum concentration are well-known [4]. However, as these efficiencies assume an “infinite stack” of solar cells and, for the concentrating devices, a concentration ratio of 46,300, they are unrealistic to implement.

Therefore, an important question concerns the requirements for making an ultra-high efficiency ($\eta > 50\%$) solar cell. There are three sets of parameters that need to be specified: the concentration ratio, the number of band gaps or effective band gaps, and the values of the optimum band gaps. The concentration ratio is determined by taking an intermediate value between the concentration ratios at which peak solar cell efficiencies have been measured and the value of existing concentrator modules. Five of the record efficiency concentrator solar cells are measured at concentration ratios between 300 to 350X [5], and there are multiple reports of concentrators operating in the region of 1000X [6,7,8]. In this paper, a 500X concentration is used as an advance on 350X, but one which has been built and measured.

To calculate the number of band gaps or effective band gaps required in the device, detailed balance modeling [4] for devices with 4 to 8 band gaps was performed using concentration of 500X and a spectrum of 6000 K. The results are shown in Table 1. The range of the band gaps required increases as expected with the number of band gaps (n). However, at high values of n , the lowest value of the band gap essentially saturates due to low available energy in the long wavelength region of the spectrum, and above $n = 5$ the spread in band gap is mainly accommodated by going to higher band gaps. If an AM1.5 spectrum is used rather than a black body spectrum at 6000K, the range of band gaps is narrower and the efficiency is higher, but the trends remain similar.

Table 1: Values of band gap and efficiency for tandems with four to eight junctions calculated at 500X with a black body spectrum at 6000K. N is the number of band gaps in the device.

n	Values of Band Gap (eV)	η %
4	0.60, 1.11, 1.69, 2.48	62.0
5	0.53, 0.95, 1.40, 1.93, 2.68	65.0
6	0.47, 0.84, 1.24, 1.66, 2.18, 2.93	67.3
7	0.47, 0.82, 1.19, 1.56, 2.0, 2.5, 3.21	68.9
8	0.44, 0.78, 1.09, 1.4, 1.74, 2.14, 2.65, 3.35	70.2

More realistic efficiencies than the efficiency limits in Table 1 can be determined by examining the ratio between experimental efficiencies and detailed balance

efficiencies for existing solar cells. For example, record Si and GaAs one-sun solar cells achieve 80- 85% of their theoretical maximum efficiencies, while Si and GaAs concentrators reach 70–80% of their theoretical efficiency [5]. Both one sun and concentrating tandems have measured efficiencies between 65–70% of their theoretical maximum. Hence, an achievable fraction of the efficiency limits is chosen as 75%. In order to achieve an overall efficiency of 50% at 500X, a theoretical efficiency of 66% is required. This corresponds to a solar cell with 6 physical or “effective” band gaps using the 6000K spectrum, or 5 using an AM1.5 spectrum. For the AM1.5 spectrum the band gaps become approximately 0.6, 1.0, 1.3, 1.7, 2.3 eV.

Once the number and values of the band gaps have been identified to achieve > 50% efficiency, the material system to most closely implement these band gaps must be determined. Figure 1 shows the available material systems, plotting the band gap and lattice constant. Existing three-junction tandems use GaInP/GaAs/Ge or GaInP/InGaAs/Ge and have achieved efficiencies of 36.9% under the Low-AOD spectrum [5, 9]. However, above 3 junctions, achieving a lattice matched device becomes increasingly difficult. Dilute nitrides [10] and mechanical stacks using the antimonide system [11] have been proposed for 4-junction devices. Increasing the number of devices to 5-junctions (which is needed to achieve > 50%) will require a device with substantial lattice mismatch. In addition, the wide band gap non-nitride III-V materials are indirect and also have lower than optimum band gaps. However, one disadvantage of the III-nitrides is that they do not have a physical band gap below 0.68 eV. However, since the low band gap device in the tandem offers relatively low voltages, tandem stacks which require band gaps below 0.68 eV may be advantageously implemented by an “effective” band gap, such as quantum well or quantum dot approaches.

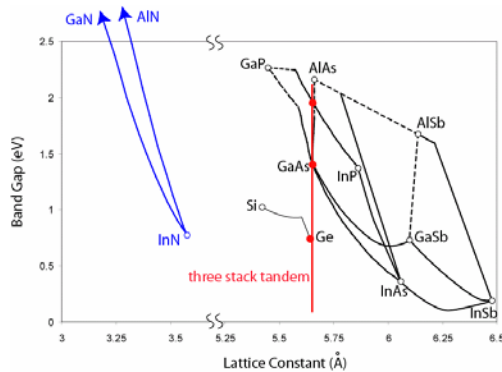


Figure 1: Lattice-band gap diagram for III-V solar cell materials, including the III-nitrides.

In addition to the direct nature of the wide-band gap materials in the InGaN material system, the InGaN material system offers several advantages including the ability to substantially cover the required band gap range with a single alloy, the apparent insensitivity of the InGaN material system to high dislocation densities and the polarization and piezoelectric properties of the material which introduce electric fields and surface dipoles that may counter the effect of dislocations and provide a new design parameter. The following sections examine properties of the III-N material system and how they can be used in photovoltaics.

3 III-N MATERIAL SYSTEM

The III-N material system, which includes AlN, GaN, InN and their alloys, has undergone remarkable development due to the use of GaN and InGaN for blue LEDs and laser diodes [12]. However the III-nitride materials mostly used for light emitters, GaN, AlN and $\text{In}_x\text{Ga}_{1-x}\text{N}$ with $x < 0.2$, were not used for solar cells due to their high band gap. InN seemed more promising, with a band gap of 1.9 eV, that could be a suitable candidate material for a two stack tandem on silicon [13]. However, as bright photoluminescence (PL) had at that time not yet been achieved from InN, the material quality seemed low for high efficiency photovoltaic devices.

In late 2001 and early 2002 Davydov et al [1], Wu et al [2] and Matsuoka et al [3] measured PL from InN films, not at 1.9 eV as expected, but at approximately 0.7 eV, thus indicating that the band gap was lower than previously thought. Given the dramatic revision in the band gap, the new measurements gave rise to considerable debate about the measurements and the mechanisms controlling the material. While some uncertainties remain [14], a substantial body of evidence points to a fundamental band gap of 0.68 eV (see Vurgaftman [15] for a review of III-nitride band parameters). Explanations for the measurements of the band gap as 1.9 eV center either on the Burstein-Moss shift which increases the effective band gap as the doping increases [16] or the incorporation of oxygen. Oxygen goes into InN as a dopant in low concentrations, but appears to form a higher band gap alloy (1.9 eV) of In_2O_3 at higher oxygen levels. The ability to convert from low band gap (0.7 eV) to high band gap (1.9 eV) by oxidizing the films [17] suggests a pivotal role of oxygen in the explanation of the band gap. While the band gap of the material is a critical material parameter, many other material parameters are critical in the ability to implement high efficiency solar cells, including the lattice constant and suitable substrates, the ability to achieve p-type doping, the absorption depth and diffusion length.

3.1 Substrates

The III-nitrides typically crystallize in a wurtzite crystal structure, unlike Si, Ge, and GaAs which crystallize in a diamond or zinc-blend structure. Sapphire is the most commonly used substrate for the growth of wurtzite GaN. However, due to the large lattice and thermal mismatches between sapphire and III-Nitrides (16% for GaN on sapphire and 29% for InN to sapphire), epitaxial films on sapphire result in dislocation densities typically in the 10^7 - 10^{10} cm^{-2} range. Other substrates are SiC and ZnO which provide better lattice match, but nevertheless have similar dislocation densities.

As an alternative to these substrates, both $\langle 111 \rangle$ oriented Si and Ge are excellent candidates for In-rich InGaN applications. Figure 2 shows the lattice match of InN to Si and Ge, which is 7.8%, 11.3%, 17% and 20.1% for InN/Si, InN/Ge, GaN/Si, and GaN/Ge respectively. Thus, Si or Ge substrates are better lattice matched to InN than traditional GaN/Si or GaN/sapphire. Additionally, very high quality Si and Ge wafers are easily available at low cost and their conductivity allows for a vertical device design that can be contacted from the front and rear.

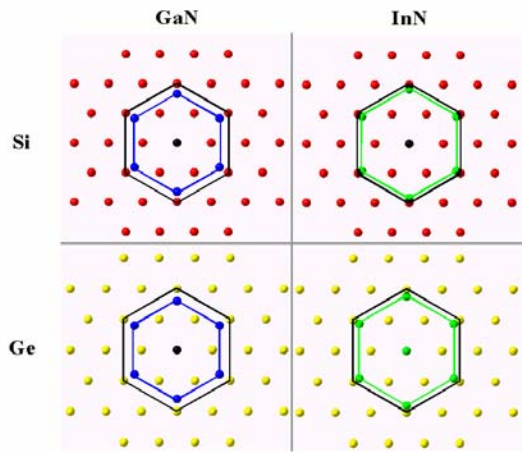


Figure 2: Calculated schematic showing the lattice structure of Si and Ge compared to InN. The Si and Ge lattice is shown as dots, with the $\langle 111 \rangle$ planes as the outer hexagonal, and GaN or InN as the inner hexagonal.

3.2 Polarization and Piezoelectric Constants

In addition to its band gap range, another unique feature of the III-nitrides is the strong polarization or piezoelectric effects [18, 19]. AlN, GaN and InN are all highly polar molecules, such that at the interface between the materials, a large dipole may develop, which alters the surface properties and induces an electric field in the bulk region between two surfaces. The spontaneous polarization is particularly strong at AlN/GaN interfaces, and less so between GaN and InN. In addition to electric fields induced by polarization, an electric field may also be induced in the material by the piezoelectric fields, which are electric fields induced by strain in the material. The piezoelectric coefficients are high in the III-nitrides, hence a substantial electric field will develop in strained material. The ability to modify the surface potentials and generate electric fields across the materials is critical in the interpretation of transport properties of the III-nitrides, and is also a new design parameter [20].

3.3 P-type doping

Achieving p-type conductivity in InGaN alloys is difficult due, in part, to a high background concentration of electrons. By improving the structural quality of GaN, p-type GaN can be achieved but one still has a limit of less than low to mid 10^{18} cm^{-3} hole concentration due to the deep activation energy of acceptors in GaN, which is approximately 160 meV for Mg in GaN, leading to approximately 1% of the incorporated Mg contributing to the hole concentration at room temperature [21]. With InGaN, it is expected that higher hole concentrations can be achieved due to a lower activation energy than for GaN. For example, the activation energies of Mg were 141 and 80 meV for 4% and 14% In mole fraction, respectively [22]. The corresponding electrical hole concentrations are 5.3×10^{18} and $1.6 \times 10^{19} \text{ cm}^{-3}$ [22].

Despite of this advantage, practical InGaN has been shown to possess higher background electron concentrations of $\sim 10^{19} \text{ cm}^{-3}$ which compensates the holes [23]. These higher background electron concentrations likely come from the growth on larger

lattice-mismatched substrates, generating shallow donors. This feature is supported by the fact that higher hole concentrations can be obtained using slower growth rates, otherwise maintaining the same growth conditions for Mg-InGaN [24]. To date, no report of p-type conductivity has been given for In \gg 32%, indicating that p-type InN may be a challenge to obtain.

3.4 Absorption Depth and Diffusion Length

The absorption depth ($1/\alpha$) and the diffusion length (L) are critical parameters in making high efficiency solar cells. The absorption coefficient is high in all of the InGaN range, and importantly increases rapidly near the band edge. The high absorption is a critical factor in achieving high collection since the absorption depth must be shorter than the diffusion length for high collection.

While the recombination properties of InGaN films are critical in determining the performance of photovoltaic devices, substantial variation in reported values exists in the literature, even for GaN, the best characterized of the materials. The recombination processes in the III-nitrides are controlled by several possible processes: excitonic recombination, radiative recombination, non-radiative, and recombination controlled by localization of carriers caused by phase separation in In-rich InGaN alloys. The reported values of B , the band-to-band radiative recombination coefficient, vary from 1×10^{-8} to $2.4 \times 10^{-11} \text{ cm}^3/\text{s}$, but are typically on the order 7×10^{-10} [25]. These values of the radiative lifetimes are consistent with those extracted from measurements [26]. However, films in general have a high non-radiative recombination component, and measured lifetimes are typically in the range of several hundred ps to 2 nsec [27, 28, 29].

The diffusion length depends on both the minority carrier lifetime and the diffusion coefficient. The majority carrier mobility for n-type material is measured as high as $845 \text{ cm}^2/\text{Vs}$ for thick epilayers, but only 5 for minority carrier in n-type and majority holes in p-type [30] and on the order of 500 for thinner layers. The low mobilities for minority carriers mean that most extracted diffusion lengths are between 0.2 to 0.8 μm , but several reports give measured diffusion lengths of over 1 μm , [27, 29,31].

InN and In-rich epilayers are less well characterized than GaN, and the characterization of the material is complicated by the phase separation of InGaN layers into small, localized regions of In-rich InGaN, which act to localize carries in a similar fashion as a quantum dot. Theoretically, InN has a lower band-to-band recombination coefficient than GaN [32] as well as having higher mobilities. The higher mobilities have been experimentally verified for majority carriers, with mobilities measured of $2200 \text{ cm}^2/\text{Vs}$. For epilayers, Chen et al measure a lifetime of 300 ps and a majority carrier mobility of $1340 \text{ cm}^2/\text{Vs}$ [33].

4 MODELLING InGaN TANDEM SOLAR CELLS

A key advantage of the InGaN material system is that using a tandem (or quantum-based) device with a large number of band gaps can be grown by varying the alloy composition. However, the efficiency of the resultant device will be strongly controlled by the practical material parameters, such as diffusion length. To

determine the efficiency potential of InGaN tandem solar cells, a material parameter set of the InGaN alloy was developed and used to model tandem InGaN solar cells.

To determine the composition of indium in the $\text{In}_x\text{Ga}_{1-x}\text{N}$ alloy, the equation, the equation relating band gap to mole fraction x is used:

$$E_G(x) = xE_{G_InN} + (1-x)E_{G_GaN} - Cx(1-x)$$

where x is the mole fraction of indium $E_{G_InN} = 0.68\text{eV}$, $E_{G_GaN} = 3.45\text{eV}$ and C is the bowing parameter and $C = 1.45\text{ eV}$ [15]. The other material parameters are taken where possible from experimental data. The details of the material parameters set are described elsewhere [34], but are summarized for InN and GaN in Table 2. The absorption coefficient data was taken from 35,36,37.

Table 2: Properties of InN and GaN used in PC1D.

Parameter	InN	GaN
Band Gap	0.68 eV	3.45 eV
Electron Affinity	6.4 eV	4.1 eV
Dielectric Constant	15.3	8.9
Mobility: Electron	2200	1000
Hole	200	5
Lifetime: Electron	500 ps	1 nsec
Hole	500 ps	5 nsec
Refractive Index	2.9	2.3
Intrinsic carrier	5.280E+12	4.455E-11

Figure 3 shows the QE for a five-stack tandem made from the InGaN material system using the material parameters from Table 2 and with the reflectivity set to zero. Figure 3 shows that high absorption coefficient allows thin a layers and high collection from the layers. The efficiency, Voc and Jsc of the modeled cells are shown in Table 3. Even for the low values of lifetime, the V_{oc} s are approximately $E_g/q - 0.4\text{ eV}$, similar to existing tandems [9].

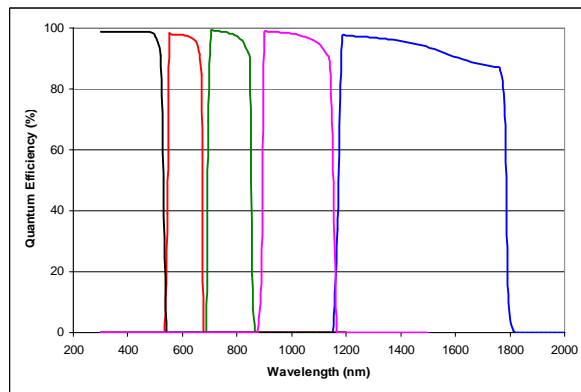


Figure 3: QE for the 5-stack tandem from PC1D.

In addition to allowing a large range of band gaps within a single alloy system, an additional advantage of the III-nitride material is their large spontaneous and piezoelectric coefficients, giving sheet charges on the order of $1 \times 10^{13}/\text{cm}^2$, and giving an additional design parameter that can be used to mitigate the non-ideal parameters of the III-N system. For example, control over the interface charge can be used to make inversion

layer devices, thus allowing solar cells without p-type doping. Using a surface charge of $-5 \times 10^{12}/\text{cm}^2$ and the parameters of Table 2 at one sun gives a solar cell with $V_{oc} = 463\text{ mV}$, $J_{sc} = 47\text{ mA}/\text{cm}^2$, $\eta = 14.9\%$.

Table 3: Modeled efficiency from PC1D of a 5 stack tandem using the parameters in Table 2.

Cell	Voltage (V)	Current (A/cm^2)	Efficiency (%)
cell 5	1.97	4.16	14.8
cell 4	1.45	4.97	12.9
cell 3	1.05	4.90	8.8
cell 2	0.64	5.92	6.0
cell 1	0.29	6.25	4.5
Total			47.0

5 InN ON Ge SUBSTRATES

The use of Ge as a substrate for InGaN-based solar cells offers multiple advantages. First, Ge is already used as a substrate material, and many of the advantages of Ge- to GaAs-based tandems are also relevant to InN solar cells, such as cost and availability. Ge also has a low band gap and can be used as an active junction, although InN has a similar band gap. A critical feature compared to other available substrates used in the III-N materials is that a vertical conduction device can be made, that Ge is thermally conductive and that a tunnel or electrical contact can be made between the layers.

$\langle 0001 \rangle$ oriented InN has been grown on $\langle 111 \rangle$ Ge directly, using AlN buffer layers, and using metallic, crystalline Al buffers. The HR-XRD measurements are shown in Figure 4. InN grown directly on Ge is of comparable quality to that grown on sapphire, InN films are highly columnar with the best 0002 ω -2 θ full width at half maximum (FWHM) values are $\sim 144\text{ arcsec}$. The best 0002 ω -scans FWHM for directly grown InN/Ge showed $\sim 2597\text{ arcsec}$, indicating significant tilt and mosaic grain structure. Growths on AlN buffers were plagued with difficulties in preventing amorphous Ge_3N_4 formation.

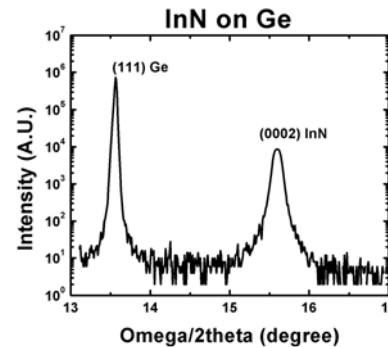


Figure 4: XRD results from InN grown on $\langle 111 \rangle$ Ge.

Crystalline Al was deposited on Ge at a thermocouple temperature of $475\text{ }^\circ\text{C}$. RHEED images confirm the formation of crystalline Al (or possibly a crystalline Al-Ge alloy) as shown in Figure 5. InN grown on these Al buffer layers showed a marked improvement, 2x, in the x-ray diffraction omega scans indicating reduced tilt and mosaic structure.

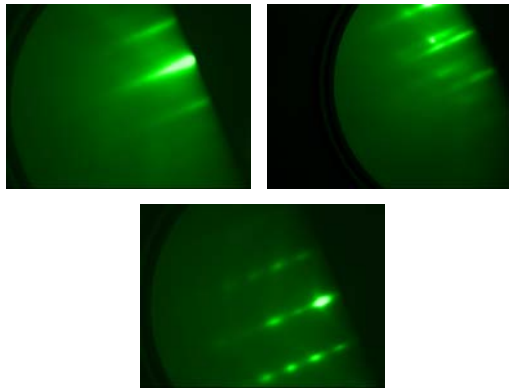


Figure 5: RHEED images. (a) Bare Ge wafer; (b) Al and Ge pattern present once Ge is exposed to Al flux. (c): InN grown on Al.

Modeling of the crystalline alignment in the Ge-Al-InN stack indicates the possibility of this crystalline Al layer acting as a buffer, accommodating the lattice mismatch via domain matching. Specifically, every seven-unit cells of Al aligns to within 0.21% to every 5-unit cells of Ge. Likewise, every 4th unit cell of InN aligns to every 5th unit cell of Al to within 1% as shown in figure 3. While this domain matching results in a high dislocation density, it also insures long-range coherence and is consistent with the columnar structure observed experimentally. In vertical conduction solar cell applications, the vertically threading dislocations may not be problematic while the ability to tandem connect several cells together with Al epitaxial interconnects will likely improve multi-junction solar cell performance.

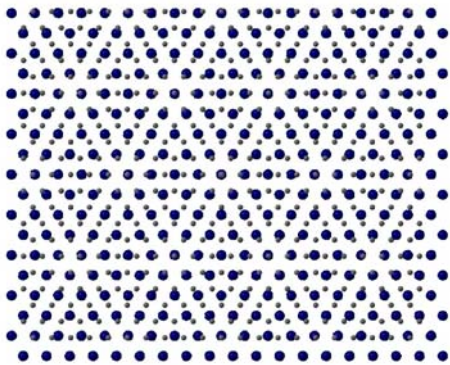


Figure 6: Superposition of Al and InN showing the domain matching. Every 4th InN lattice point aligns with every 5th Al lattice point.

6 HIGH BAND GAP InGaN SOLAR CELLS

The substantial development of the high-band gap GaN and InGaN alloys and QW devices offer the opportunity to experimentally examine the potential of the III-nitrides. A GaN device and a QW p-i-n device with the QW layer consisting of with 5 $\text{In}_x\text{Ga}_{1-x}\text{N}$ QWs with $x = 0.08$ in the i-region were grown and processed into solar cells. The device structure of the GaN p-i-n is shown in Figure 7. While the band gap of GaN is too high ($E_g = 3.45$ eV) for solar applications, the use of the GaN material ensures that the collection efficiency is not affected by phase separation in InGaN layers.

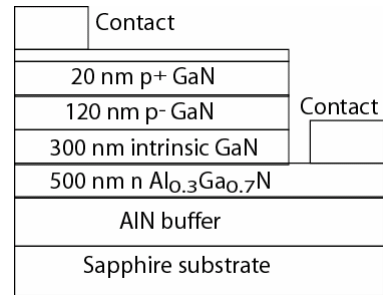


Figure 7: Device structure of the GaN p-i-n solar cell.

As both the devices respond either in the UV or in the blue/violet region of the visible spectrum, a mercury arc lamp is used to measure the IV curves of the devices. Both devices displayed similar J_{sc} 's, but the GaN device has a non-ohmic contact that prevents measurement of Voc. The IV curve for the QW solar cell is shown in Figure 8.

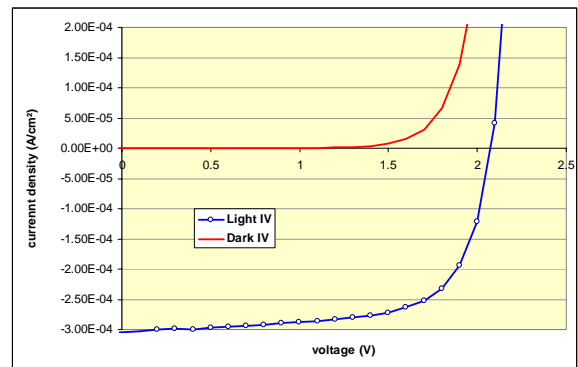


Figure 8: IV curve using a mercury lamp of QW InGaN solar cell.

The spectral response curves (in arbitrary units) of the GaN p-i-n and GaN/InGaN QW solar cells are shown in Figure 9 and Figure 10. Due to its relatively high band gap, the GaN spectral response is measured with a deuterium lamp. The QW GaN/InGaN devices is measured using a xenon lamp. Both sources were not calibrated, but the external quantum efficiency is estimated as 30% for both devices. Both the devices were measured from the rear, reducing the quantum efficiency due the partial absorption of light in the p-layers, rather than passing through the high band gap buffer.

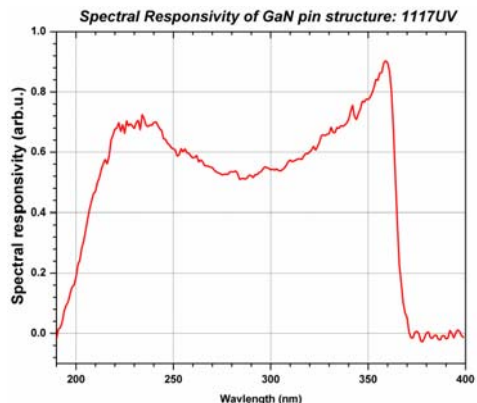


Figure 9: Spectral response of p-i-n GaN solar cell (arbitrary units).

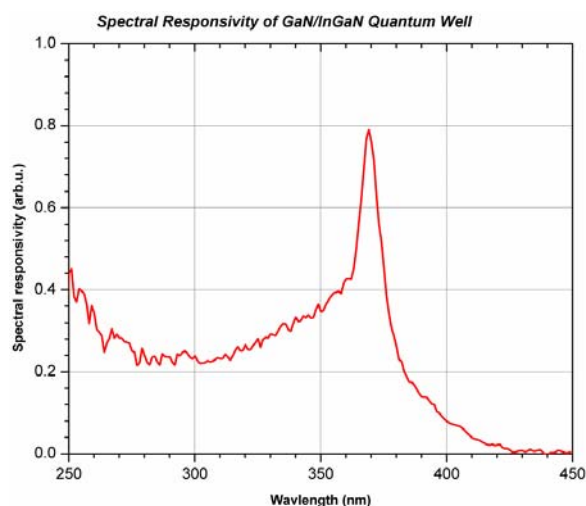


Figure 10: Spectral response of the QW solar cell.

7 CONCLUSIONS

The InGaN material system has several unique properties, particularly the wide range of band gaps over the alloy composition and the polarization properties that make it suitable to ultra-high efficiency photovoltaics. Using measured material parameters where available, PC1D modeling shows that a 5-stack tandem at 500X approaches 50% efficiency. Experimental results of InN films grown on Ge show a crystalline Al interlayer, which can be used to replace tunnel junctions. Experimental results on high band gap InGaN QW solar cells (3.1 eV), show open circuit voltages of 2.1 V, and estimated external QW of > 30%.

8 ACKNOWLEDGEMENTS:

The authors would like to thank Jayantha Senawiratne from Georgia State University for the spectral response measurements.

This work was partially supported by U.S. D.O.E. and the National Renewable Energy Laboratories, monitored by Dr. Robert McConnell and Dr. Martha Symko-Davies and the Office of Naval Research, monitored by Dr. Colin Wood.

REFERENCES

- [1] V. Yu. Davydov, et al., *Physical Status Solidi B*, 229, 3, p. R1-R3, (2002).
- [2] J. Wu, W. Walukiewicz, K.M. Yu, J.W. Ager, E.E. Haller, and Schaff, W.J. Hai Lu, *Applied Physics Letters*, 80, 25, p. 4741-3, (2002).
- [3] T. Matsuoka, H. Okamoto, M. Nakao, H. Harima, and E. Kurimoto, *Applied Physics Letters*, 81, 7, p. 1246-8, (2002)
- [4] A. Devos, "Endoreversible Thermodynamics of Solar Energy Conversion", OUP, 1992.
- [5] K. Emery, D.L. King, S. Igari, W. Warta, M.A. Green, *Progress in Photovoltaics*, 12, 1, 55-62, (2004).
- [6] S.R. Kurtz, and D.J. Friedman, AIP Conference Proceedings, 462, p. 378-84, (1999).
- [7] J.M. Gordon, E.A. Katz, D. Feuermann, and M. Huleihil, *Applied Physics Letters*, 84, 18, 3642-4, (2004).
- [8] M.J. O'Neill, A.J. McDaniel, and P.A. Jaster, Proc. 29th PVSC, 1369-72, (2002).

- [9] R. R. King, et al, *3rd World Conference on Photovoltaic Energy Conversion*, Japan, (2003).
- [10] J.F. Geisz, and D.J. Friedman, *Semiconductor Science and Technology*, 17, p. 769-777, (2002).
- [11] C. Agert, P. Lanyi, O.V. Sulima, W. Stolz, and A.W. Bett, *IEE Proceedings-Optoelectronics*, 147, 3, p. 188-92, (2000).
- [12] S. Nakamura, S. Pearton, G. Fasol, "The blue laser diode, 2 ed", Springer Verlag 2000.
- [13] T. Yamaguchi, C. Morioka, K. Mizuo, M. Hori, T. Araki, A. Suzuki, and Y. Nanishi, *2003 International Symposium on Compound Semiconductors*, 2003, p 10-11, (2003)
- [14] T.V. Shubina, et. a, *Physical Review Letters*, 92, 11, p. 117407, (2004)
- [15] I. Vurgaftman, and J.R. Meyer, *Journal of Applied Physics*, 94, 6, 15, p 3675-96, (2003)
- [16] W. Wu, W. Walukiewicz, *Superlattices and Microstructures*, 34, p. 63-75, (2003).
- [17] M. Hangyo, H. Harima, M. Yoshimoto, T. Yamaguchi, T. Araki, Y. Nanishi, and K. Kisoda. E. Kurimoto, *Appl. Phys. Lett.* 84(2) 212 (2004)
- [18] F. Bernardini, and V. Fiorentini, *Physical Review B*, 64, 8, 085207/1-7, (2001).
- [19] V. Fiorentini F. Bernardini, *physica status solidi (b)*, 216, 1, p. 391-398, (1999).
- [20] O. Ambacher et al., *Journal of Applied Physics*, 85, 3222 (1999).
- [21] T. Tanaka and A. Watanabe, H. Amano, Y. Kobayashi, I. Akasaki, S. Yamazaki and M. Koike, *Appl. Phys. Lett.*, 65, 5, pp. 593-594 (1994)
- [22] K. Kumakura, T. Makimoto and N. Kobayashi, *Jpn. J. Appl. Phys.* 39, 4B, pp L337-L339 (2000)
- [23] W. Geerts, J.D. Mackenzie, C.R. Abernathy, S.J. Pearton, and T. Schmiedel, *Solid-State Electronics*, 39, 9, pp 1289-1294 (1996)
- [24] K. Kumakura, T. Makimoto, and N. Kobayashi, *Journal of Crystal Growth*, 221, 267-270 (2000)
- [25] O. Brandt, H.-J. Wünsche, H. Yang, R. Klann, J.R. Müllhäuser, and K.H. Ploog, *Journal of Crystal Growth*, 189/190, 790-793, (1998).
- [26] Y. Narukawa, S. Saijou, Y. Kawakami, S. Fujita, T. Mukai, and S. Nakamura, *Applied Physics Letters*, 74, 4, p. 558-560, (1999).
- [27] A. Matoussi, et al, *phys. stat. sol. (b)* 240, 1, 160 – 168 (2003).
- [28] Z.Z. Bandić, P.M. Bridger, E.C. Piquette, and T.C. McGill, *Journal of Applied Physics*, 72, 24. 3166-3168, (1998).
- [29] L. Chernyak, A. Osinsky, and A. Schulte, *Solid-State Electronics*, 45, 9, p 1687-702, (2001).
- [30] Z.P. Gaun, J Z Li, G Y Zhang, S X Jin, and X M Ding, *Semicond. Sci. Technol.*, 15, 1, (2000) 51-54
- [31] A. Vertikov, I. Ozden, and A.V. Nurmikko, *Appl. Phys Lett.* 74 ,(6) 1999, p 850-2.
- [32] A. Dmitriev, and A. Oruzhenikov, *Journal of Applied Physics*, 86, 6, (1999), 3241.
- [33] F. Chen, A.N. Cartwright, W.J. Schaff, H. Lu, *Applied Physics Letters*, 83, 24, 4984-6, (2003)
- [34] C. Honsberg, O. Jani, to be published
- [35] Yu. Davydov, et. al, *phys. stat. sol. (b)*, 229, 3, R1-R3 (2002).
- [36] J.F. Muth, et al, *Applied Physics Letters*, 71, 18, 2572-2574, (1997).
- [37] J. Wu et al, *Applied Physics Letters*, 80, 25, 24 4741-3, (2002).